Structural and electronic characterization of the MgO/Mo(001) interface using STM

H. M. Benia, P. Myrach, N. Nilius[*]*, H.-J. Freund*

Fritz-Haber-Institut der MPG

D-14195 Berlin, Germany

The nucleation and growth of ultrathin MgO films on Mo(001) has been investigated with scanning tunneling microscopy and spectroscopy. In the initial growth stage, the MgO forms rather uniform islands with rectangular shapes and defined orientation. This behavior reflects a preferential binding of the oxide O ions to the top positions in the Mo support, which can be realized only in confined areas due to the MgO/Mo lattice mismatch. At monolayer coverage, a characteristic square pattern becomes visible in the STM, indicating the formation of an MgO/Mo coincidence lattice. In the coincidence cell, the interface registry alternates between O and Mg ions being in Mo top positions. The resulting imaging contrast in the STM is dominated by a work-function modulation and not by a topographic effect, as demonstrated with STM-conductance and light-emission spectroscopy. The modulated work function in the coincidence cell is assigned to a small buckling of the oxide film with either O or Mg ions being closer to the Mo surface.

Keywords:

Oxide thin films, nucleation and growth, coincidence lattice, MgO, Mo, Scanning tunneling microscopy and spectroscopy

[*] Corresponding author: nilius@fhi-berlin.mpg.de

Introduction

Thin oxide films have attracted a lot of attention in recent years due to their importance in the materials sciences, in microelectronic and heterogeneous catalysis. Oxide films are utilized in these fields as protective coatings against corrosion, as dielectric spacer layers and electron-transparent model systems for insulating bulk oxides. Such applications heavily depend on the possibility to prepare homogeneous films without holes even if the film thickness is reduced to a few atomic layers. Only a structurally intact film guarantees the desired properties and prevents mis-operation, for instance due to pit corrosion, dielectric breakthroughs, or parasitic effects originating from the support material.

Thin oxide films on metal substrates are also ideally suited to study the fundamental properties of metal-oxide interfaces.[1,2,3] Their behavior depends on various structural and electronic parameters, such as the lattice mismatch between the two systems, the atomic registry at the interface and the strength of the metal-oxide adhesion. Many theoretical attempts have been made to investigate the properties of metal-oxide interfaces; however, most of these studies are restricted to idealized and defect free systems.[4,5,6] In particular, the role of the lattice mismatch is often neglected and support and oxide layer are artificially forced to the same lattice constant. As a consequence, crucial properties of a metal-oxide system might not be accessible to the calculations, for instance if imposed by an incommensurate relationship between ad-layer and support or by large coincidence structures. Furthermore, the numerous restructuring processes of thin-film systems to release misfit-induced lattice strain cannot be treated in a satisfactory manner. However, structural relaxation that enforces the formation of dislocations,[7,8,9] mosaics[10,11] and 3D islands[12,13] governs not only the morphology of thin oxide films but also its electronic and chemical behavior.

From the experimental side, even complex metal-oxide systems can be explored with surface science techniques that are sensitive to structural and electronic aspects of the interface.[14,15] Scanning tunneling microscopy (STM) plays hereby a particularly important role, as it enables a real-space investigation of interfacial properties and dominant relaxation mechanisms in thin-film systems.[16,17,18] The STM provides insight

into the atomic morphology of an interface, but also its electronic and optical behavior can be probed via differential conductance and light emission spectroscopy.[8,19,20,21]

This paper discusses the structural and electronic characteristics of an ultrathin MgO film grown on a Mo(001) surface.[7,22,23] The MgO/Mo system is interesting for many aspects. Due to the high melting point of the Mo substrate, the oxide layer can be thoroughly annealed and pushed into its thermodynamically favored configuration. The large lattice mismatch of 5.4 % between MgO and Mo(001) enforces complex structural relaxations, which involve the insertion of an interfacial dislocation network and the formation of screw dislocations and mosaics in the film. The thickness-dependent relaxation behavior of the MgO/Mo film has been investigated with STM and diffraction techniques before.[23] Also from an electronic point of view, the system offers a number of unique properties. The oxide formation induces a considerable decline of the Mo(001) work function,[24,25] which in turn enables charge transfer processes from the metal into adsorbates on the oxide surface.[26] This effect has already been demonstrated for MgO/Ag(110) films,[27] but is expected to be much larger on the MgO/Mo system due to a larger interfacial coupling in this case.[26,28]

This paper focuses on the properties of sub-monolayer and monolayer (ML) MgO films, as their quality decisively influences the growth of thicker oxide layers. It discusses in particular the effect of the lattice mismatch on the structural and electronic properties of the MgO-Mo interface. Furthermore, regular work function modulations on the surface of thin MgO/Mo films are identified as the origin for the distinct imaging contrast and spectroscopic response of the system in the STM.

II. Experiment

The Mo(001) surface used as support for the oxide preparation is cleaned by Ar^+ sputtering, annealing in an O_2 ambience and flashing to 2300 K. This procedure is repeated until a sharp (1×1) LEED pattern without super-structure spots is obtained (Fig.1). MgO films of up to two ML thickness are then produced by Mg deposition from a Mo crucible in 1×10^{-7}mbar O_2 at 300 K sample temperature. The deposition rate is set

to 1 ML/min. After deposition, the film is annealed for 10 min in UHV at the temperatures specified in the following discussion. Averaging structural information is obtained from Low-Energy Electron Diffraction (LEED) performed with a two-grid LEED optic. Real space data is acquired with a custom-built Beetle-type STM operating at liquid nitrogen temperature (100 K). The microscope is equipped with an optical read-out that consists of two parabolic mirrors and allows detection of photons emitted during the tunnel process.[29] The photons are either collected by a CCD detector attached to a grating spectrograph or by a photo-multiplier tube that measures the integral photon yield. By these means, the wavelength distribution of the emitted light or alternatively the spatial localization of emission centers on the surface can be studied.

III. Results and discussion

(A) Sub-monolayer MgO films

Figure 1 presents an STM image-series of a sub-monolayer MgO film on Mo(001), being deposited at 300 K and annealed to the indicated temperatures *T*. The as-grown film (*T* = 300 K) produces featureless and diffuse STM images and shows a faint (1×1) LEED pattern, indicating its amorphous or short-range ordered structure (not shown). This behavior is maintained until the annealing temperature exceeds 700 K, when small nano-crystallites of uniform height emerge in between the amorphous patches. Their height amounts to ~2.0 Å when measured above 3.0 V sample bias, suggesting the formation of mono-layer high MgO islands. With increasing temperature, the crystalline regions grow on the expense of the disordered patches that finally disappear at around 850 K. Simultaneously, the oxide film partially de-wets the substrate and the Mo(001) surface is exposed again. For $T > 950$ K, the MgO islands undergo an ordering process, in which they transform into uniform stripes of ~50 Å width running along the Mo[110] directions. Around 1050 K, the stripes coalesce into large irregularly shaped oxide patches, most likely due to Ostwald ripening. Furthermore, the MgO starts desorbing from the surface and larger regions of bare Mo(001) become visible. Above 1100 K, the oxide film has finally disappeared and only small randomly-shaped islands remain visible. It should be noted that the MgO desorption temperature sensitively depends on the initial oxide

coverage and sub-monolayer structures evaporate at considerably lower values than thick films. [30]

The ordering process of the MgO film observed by STM is also found with LEED. A LEED pattern with sharp Mo(1×1) reflexes surrounded by four [110]-oriented satellites shows up only for annealing temperatures above 700 K (Fig. 1, inset). The absence of a genuine MgO-induced superstructure hereby indicates that the primitive cells of oxide and support coincide and the MgO exposes a (001) surface as well. Furthermore, the MgO[100] direction needs to align with the Mo[110], as only in this configuration the lattice parameters are comparable.[23] The satellites have a fixed, energy-independent separation from the fundamental Mo spots on the LEED screen, suggesting that they are not related to a superstructure but originate from tilted oxide patches (mosaics). In this case, the distance between the satellites changes linearly with energy in reciprocal space, but remains constant on the screen. From the separation between the satellite spots, the mosaic tilt angle is determined to be 5° in the monolayer film. These findings are in general agreement with early data in the literature.[8,23]

The annealing series in Fig. 1 indicates that sub-monolayer MgO films do not form large compact islands even after prolonged thermal treatment, but break up into small oxide patches. These islands are surprisingly uniform in size and orientation, as evident in the STM image in Fig. 2a. They have rectangular shapes with edges aligned to the orthogonal Mo[110] directions and a center-to-center separation between adjacent islands of (55±5) Å. A height profile taken along a [110]-oriented line reflects the long-range order of the surface pattern (Fig. 2b). Apart from the gap marked by the arrow, the MgO islands have a regular spacing of roughly 55 Å. A closer look suggests that also the length of the islands obeys a certain discretization with one unit being close to 55 Å as well. Apparently, the sub-monolayer MgO film is composed of regular building blocks with distinct square shape (see Fig. 2a).

A comparison of the MgO(001) and Mo(001) lattice constants sheds light on the nature of this distinct morphology. The mismatch amounts to 5.4%, ($d_{Mo\text{-}Mo}$ = 3.15 Å versus $d_{O\text{-}O}$ = 2.98 Å), which is too large for the pseudo-morphic growth of a complete oxide layer. As a consequence, the sub-monolayer film breaks apart into small islands, in which a

favorable MgO/Mo registry can be stabilized. The main binding contribution between MgO and Mo is the interfacial coupling between the oxide O ions and the Mo atoms, whereby the O preferentially occupies top sites on the metal surface.[26,31,32] This binding configuration will thus be realized in the middle of the square MgO islands (Fig.3a). Due to the lattice mismatch, the O atoms are gradually displaced from the top positions and pushed towards Mo bridge and hollow sites with increasing distance from the center. Simultaneously, the Mg atoms move away from the preferred hollow to bridge and top positions. This change in registry is associated with a considerable weakening of the interfacial MgO/Mo bonds, as reflected by a larger metal-oxide distance. According to DFT calculations for the comparable MgO/Pd system, the bond length increases from 2.38 Å for O in Pd top positions to 2.96 Å for Mg atoms bound atop.[4] A substantial repulsion between the Pd and Mg ion cores has been identified as the origin of the bond lengthening and the concomitant reduction of the metal-oxide adhesion. A similar weakening of the interfacial coupling is expected for the MgO/Mo system when Mg atoms are forced to occupy unfavorable Mo top sites. This binding configuration is therefore avoided during the growth of sub-monolayer films and the respective surface regions are left open (Fig. 3a). As a result, the MgO forms uniform square islands, whose size reflects the energy balance between filling unfavorable adsorption sites upon growth and nucleating new islands. For the experimentally determined MgO building blocks of ~55×55 $Å^2$ size, the O atoms are displaced from their preferred top positions by a maximum of ~1.7 Å. This value has to be taken as upper bound, because the bulk MgO lattice constant will be expanded in the monolayer film in order to reduce the mismatch with the Mo surface. Also the mosaicity of the sub-monolayer film can in parts be explained by changes in the interfacial registry. Using the bond-length modulations computed for the MgO/Pd system (0.58 Å), a tilt angle below 2° is calculated when going from an O-Mo to a Mg-Mo stacking configuration, which is smaller than the value extracted from LEED.

In summary, the disruption of sub-monolayer MgO films into regular square patches arises from the avoidance of unfavorable stacking configurations at the metal-oxide interface. The corresponding surface regions are left open, which gives rise to the formation of square islands. With increasing MgO exposure, those sites have to be filled

eventually to produce a compact oxide film. The underlying processes are described in the next section.

(B) Monolayer MgO films

Increasing the nominal MgO thickness to one ML and annealing the sample to 1000 K leads to the development of a closed oxide film. Its surface is covered by a square pattern with (55±5) Å periodicity that remains visible in the STM for up to 5 ML thick films (Fig. 4a). The apparent corrugation of this square lattice amounts to 0.8 Å for the optimal imaging conditions at 4.0 V. In addition, randomly-oriented dark lines are detected that are assigned to domain boundaries between adjacent MgO patches. Surprisingly, the lines of the square pattern are tilted by 45° with respect to the island edges in sub-monolayer films and follow the Mo[100] directions, although the associated length scale remained the same. The 45° tilt of major MgO elements is not reflected in the LEED pattern, which still displays [110]-oriented satellites that are indicative for a certain film mosaicity (Fig. 4a).[8] The derived tilt angles decrease however from 5° in the monolayer film to 1.5° in films of 6 ML thickness. Furthermore, the central spot of each reflex disappears for certain combinations of film thickness and electron energy, suggesting an out-of-phase scattering-condition between MgO regions of different topographic height.[33] The superstructure pattern on the MgO surface that is clearly visible in the STM does not show up in electron diffraction, most likely due to the limited coherence length of our LEED system. It produces however pronounced extra spots in gracing-incidence X-ray diffraction (GIXD), as discussed in Ref. [23].

The interpretation of the line pattern observed on compact MgO/Mo(001) films closely follows the one of the square islands at sub-monolayer coverage. Using the bulk mismatch of 5.4%, the unrelaxed MgO forms a coincidence lattice with the Mo surface, whereby 19 MgO unit cells overgrow 18 Mo cells. The resulting lattice parameter of the superstructure calculates to 56.6 Å, in close correspondence to the periodicity of the line pattern. The use of the MgO bulk parameter is justified in this case, as GIXD finds only a ~1% expansion of the monolayer MgO lattice with respect to the bulk value.[23] A structure model of the coincidence cell is depicted in Fig. 3b. In the center, the O atoms

occupy Mo top sites (Mg in hollow sites) as in the sub-monolayer film. When moving towards the edges and corners of the cell, this favorable binding configuration is replaced by O atoms in Mo bridge and hollow positions, respectively. This shift of the interfacial registry is again associated with an increase of the MgO/Mo interlayer distance. The monolayer MgO films thus experiences a considerable buckling on the Mo surface, whereby the elevated areas coincide with the Mg-Mo stacking regions at the edges and corners of the coincidences. These height modulations are partially responsible for the observation of the line pattern on the MgO surface. However, we will demonstrate later that the visibility of the superstructure in the STM strongly depends on the imaging bias and has therefore an electronic contribution.

The directions of maximum slope in the buckled MgO film run from the center to the corners of the coincidence cell (see arrows in Fig.3b) and therefore along the Mo[110] directions. These tilt directions are compatible with the orientation of the LEED satellites, verifying their connection to the mosaicity in the oxide film. The changes in interfacial registry cause considerable strain modulations in the film, with tensile and compressive contributions dominating in the Mg-Mo and O-Mo stacking regions, respectively. With increasing distance from the interface, the strain distribution quickly homogenizes, enabling the film to flatten out. The subsequent removal of the mosaicity is in good agreement with the vanishing LEED satellites observed for thicker films.[7,8] For a film thickness above 8 ML, no sign of the registry modulation at the interface is observed any more, while the residual misfit strain is released via domain boundaries and screw dislocations in the film. A comprehensive discussion of the strain release in the MgO/Mo system can be found in the literature.[23]

Further support of the structure model proposed for the MgO/Mo interface comes from an analysis of the defect structure of the film (Fig.4b). Besides randomly oriented line defects, various point defects are detected in well-resolved STM images being either O/ Mg vacancies or small vacancy clusters. They can be divided into three groups according to their position in the coincidence cell. More than half of the lattice defects are found along the bright lines (see dot in Fig. 4b as an example); while roughly a quarter emerges at the crossing points of two lines (square) and in the dark regions in between (triangle). Normalizing these values to the total number of atomic sites in the respective areas

reveals that 64% of the defects are located at the line intersections, while only 34% and 2% are inserted along the lines and in the central part of each coincidence cell, respectively (Fig.4b). This result corroborates the model of Fig. 3b. Along the bright lines and in particular at their crossing points, the O atoms occupy energetically unfavorable bridge and hollow sites, which lowers the thermodynamic stability of these particular oxide regions. They are consequently more susceptible to the formation of lattice defects than the centers of the coincidence cell having a favorable O-Mo registry.

(C) Electronic properties of monolayer MgO films

According to the previous paragraph, the square pattern on the MgO/Mo surface can be related to an alternation of more (O-Mo) and less-favorable (Mg-Mo) binding configurations at the interface. The mechanism that gives rise to the visibility of the coincidence structure in the STM is however not yet clear. To explore a possible electronic origin of the contrast, the oxide surface has been imaged at different sample bias (Fig. 5). At low positive bias (2.4 V), a heavily corrugated, apparently disordered surface is revealed with no indication for the coincidence lattice. With increasing bias, the overall corrugation decreases and domain boundaries become visible as dark lines in the oxide surface. The characteristic square pattern appears rather suddenly at 3.5 eV and remains detectable only in a relatively small bias window. Already above 4.5 V, the surface corrugation increases again and the line pattern vanishes (Fig. 5a).

The pronounced bias dependence of the MgO appearance indicates a large electronic contribution to the STM imaging contrast that even exceeds the effect of the geometric buckling. Between 2.4 and 3.1 V, especially those oxide regions turn bright that exhibit a low-lying conduction band and therefore a high final-state-density for electron tunneling from the tip.[34,35] The band onset in ultrathin MgO films has been determined as 2.5 V via conductance spectroscopy.[19,20] However this value is subject to large spatial modulations due to a partial oxidation of the Mo surface and a resulting chemical inhomogeneity of the metal-oxide interface. With increasing bias, the surface corrugation becomes smoother, as the conduction band is reached by the tunneling electrons everywhere in the film. The only exceptions are the randomly oriented domain boundaries that still appear

with reduced topographic height. A new contrast mechanism emerges for bias values higher than the work function of the system, when electron tunneling is replaced by field emission transport through the oxide film.[36] In the field emission regime, electrons leave the classically-forbidden tunnel barrier and penetrate the vacuum region between tip and sample through which they propagate as free carriers with a defined wavelength. Whenever multiples of half the electron wavelength match the geometrical distance between vacuum barrier and sample surface, standing electron waves with a high electron transmissibility develop, the so called field emission resonances (FERs). Their energy position is mainly governed by the local sample work function ϕ, which sets the bottom of the classically accessible part in the STM junction.[37] If ϕ varies across the surface, large modulations in the image contrast occur due to the different contributions of the FERs to the electron transport.[19,21] The fact that the oxide square pattern appears in the STM around the reported work-function values of the MgO/Mo system (3.3-3.9 eV)[25,38] now suggests a FER and hence work-function mediated imaging contrast.

This assumption is verified by measuring the bias position of FERs at different regions of the coincidence cell via dz/dV spectroscopy (Fig. 5b). The lowest FER is detected at 3.9 V along the edges of the coincidence cell. It is responsible for the appearance of bright lines in the STM images taken around 4.0 V, because the resonance drastically increases the junction conductance.[21,24] The FER shifts to 4.2 V in the center of the coincidence cell, which consequently remains dark in low-bias images. Not surprisingly, the contrast fades away in images taken well above 4.2 V, as the lowest FER is reached throughout the coincidence cell and the conductance becomes homogeneous again. The down-shift of FERs above the bright lines indicates a lower work function of the Mg-Mo compared to the O-Mo stacking regions, an effect that would be compatible with a buckling of the MgO film on Mo(001). In the line regions, a positive surface dipole is created because the Mg^{2+} ions on Mo top sites are farther away from the interface than the O^{2-} ions in the hollow positions. In the center of the coincidence cell, on the other hand, the surface dipole is more negative as the top-bound O^{2-} ions are more elevated than the hollow-bound Mg^{2+} species. The associated effect on the work function causes a downshift of the FERs positions above the Mg-Mo regions, but to an up-shift on the O-Mo patches, giving rise to the distinct imaging contrast around 4.0 V. It should be noted that this

interpretation does not include the interfacial dipole that evolves from a charge transfer between oxide and metal support and is of opposite sign for monolayer oxide films.[4,39] This dipole also varies when going from the O-Mo to the Mg-Mo stacking region due to the different interlayer distances, an effect that might even compensate the influence of the MgO rumpling. In fact for the Pd/MgO system, a slightly lower ϕ value has been calculated for the O-Pd stacking region, reflecting the dominance of the interfacial dipole in this case.[4] Explicit calculations for the two registries of the MgO/Mo(001) system are not available at this moment.

To quantify the work-function difference in the MgO/Mo coincidence cell, not only the first but also higher FERs need to be analyzed.[21,37] However, frequent tip changes at high voltages prevented the recording of wide-range FER spectra and therefore an accurate determination of the local work function. It should be noted that the MgO film in general reduces the work function of the Mo(001) surface and the spatial modulation due to changes in the interface registry are only superimposed to this.[25]

(D) Photon-emission behavior of monolayer MgO films

Additional evidence for the work-function modulation in the monolayer MgO film is obtained from photon-emission experiments with the STM. For this purpose, electrons with different energies are injected into the film and the emitted radiation is detected either in a wavelength-sensitive scheme (spectroscopy) or as a function of the tip position (photon mapping).[40] A spectral series taken for different excitation voltages is shown in Fig. 6a. The emission starts at 3.6 V sample bias with a weak photon peak at 980 nm (1.2 eV), and continuously blue-shifts and gains intensity with increasing excitation bias. Above 5.0 V, the final wavelength position at ~500 nm (2.48 eV) is reached and the emission intensity declines again. Additionally, a second peak emerges at 750 nm (1.65 eV) above 4.0 V excitation bias, runs through an intensity maximum and disappears again around 5.0 V without changing its spectral position (red line in Fig. 6a). Both peaks have been observed for thicker MgO films before and were assigned to (i) tip-induced plasmons (TIP) excited via inelastic electron tunneling and (ii) radiative electron transitions involving FERs in front of the MgO surface.[20,24] TIP modes are collective

electronic excitations in the coupled electron gases of tip (here Ag) and sample (here Mo) and give rise to the bias-dependent emission peak.[40,41] The yield of TIP-mediated light emission depends, among other effects, on the state density in the sample surface at the energy of the inelastic electrons that have excited a plasmon.[42] Figure 7a shows a photon map of the MgO film taken in the bias window of TIP excitations (4.0 V) together with the respective topographic image. Apparently, the emission centers are randomly distributed on the surface and show no correlation with the coincidence cell. The surface regions with high emission yield match however the bright areas in topographic images taken at 2.4 V, which is the energy of inelastic electrons after plasmon excitation (eV_o-$\hbar\omega_{plas}$). Therefore, the state density in the MgO film at the conduction band onset is responsible for the emission contrast in the TIP regime and the coincidence cell remains invisible. With a similar argument, the absence of the line pattern was explained in low-bias STM images that probe the elastic transport channel (Fig.5).

On the other hand, photon maps taken at 4.2 V reveal the square symmetry of the MgO/Mo coincidence lattice (Fig.7b). At this excitation bias, the light emission is governed by radiative electron transitions between the first FER and MgO states around the conduction band onset.[20] Such a mechanism is corroborated by the energy of the emitted photons (1.65 eV) that matches the difference between the first FER (~4.0 V) and the band onset (~2.5 V). On the Mg-Mo stacking region, the FER is fully accessible for electron transport because the resonance position (3.9 eV) is slightly smaller than the excitation bias (4.2 eV). On the O-Mo region, in contrast, only the rising rail of the first FER is reached (Fig. 5b). As a consequence of the different accessibility of the FER, the emission cross section is slightly modulated within the coincidence cell and the characteristic square pattern becomes detectable. The super-structure pattern remains however faint in the photon maps, because FER-induced emission strongly interferes with the TIP channel that is insensitive to the work function. Besides the square pattern, the domain boundaries in the MgO film show up as dark lines in the FER-mediated emission channel, indicating a pronounced shift of the FERs around such line defects. Earlier work revealed up-shifted resonance positions and hence a higher work function at the domain boundaries, which could be explained with an O-rich stoichiometry along the defect lines.[20,24]

IV. Conclusion

The formation of rectangular islands with distinct dimensions is observed for sub-monolayer MgO films grown on the Mo(001) surface. The island size is governed by the avoidance of an energetically unfavorable interface registry, in which the Mg ions of the film would sit atop the Mo surface atoms. With increasing film thickness, also those regions are filled and an MgO/Mo coincidence lattice is formed whose lattice parameter is determined by the mismatch between the bulk Mo and MgO lattice constants. Regions with Mg-Mo registry are hereby identified by their increased apparent height in the STM images. The underlying contrast mechanism is assigned to a work-function modulation in the MgO/Mo coincidence cell that can be probed by imaging the surface in the field-emission regime at elevated bias. This conclusion is supported by photon emission experiments with the STM, where the dominant emission mechanism can be switched between a state-density and a work-function sensitive channel. The characteristic superstructure appears exclusively in the latter one, emphasizing the importance of work-function modulations for the observation of the coincidence lattice.

Due to its regular work-function changes, the misfit-induced MgO/Mo coincidence lattice might be a suitable template for the spatially ordered arrangement of adsorbates. Ideal candidates are hereby molecules and adatoms with high polarizability, whose binding behavior would be sensitive to the local work function.[43] Potential self-organization processes on the MgO/Mo system are currently under investigation.

Acknowledgment

We are grateful to Stefania Benedetti for many discussions. The work has been supported by the COST action D41.

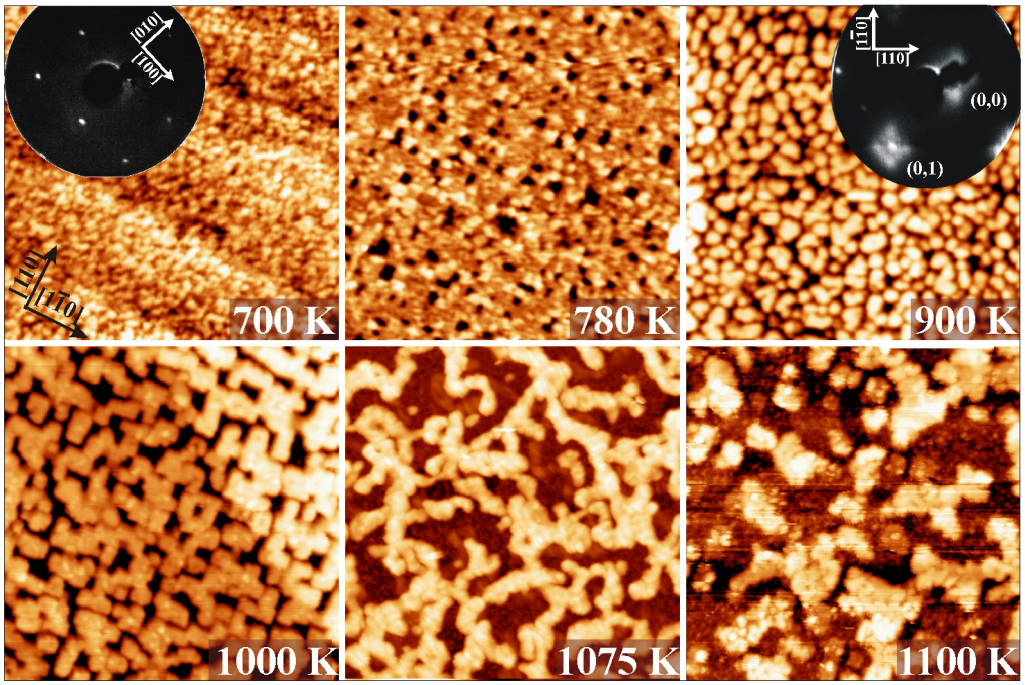

Fig.1: STM series of a sub-monolayer MgO/Mo(001) film deposited at 300 K and annealed to the indicated maximum temperatures for 10 min (U_s = 2.5-3.5 V, 100 × 100 nm^2). The left and right insets show LEED patterns of the bare Mo support (120 eV) and the MgO film after annealing to 900 K (55 eV), respectively. The four satellites around the MgO reflexes indicate the mosaicity of the oxide film.

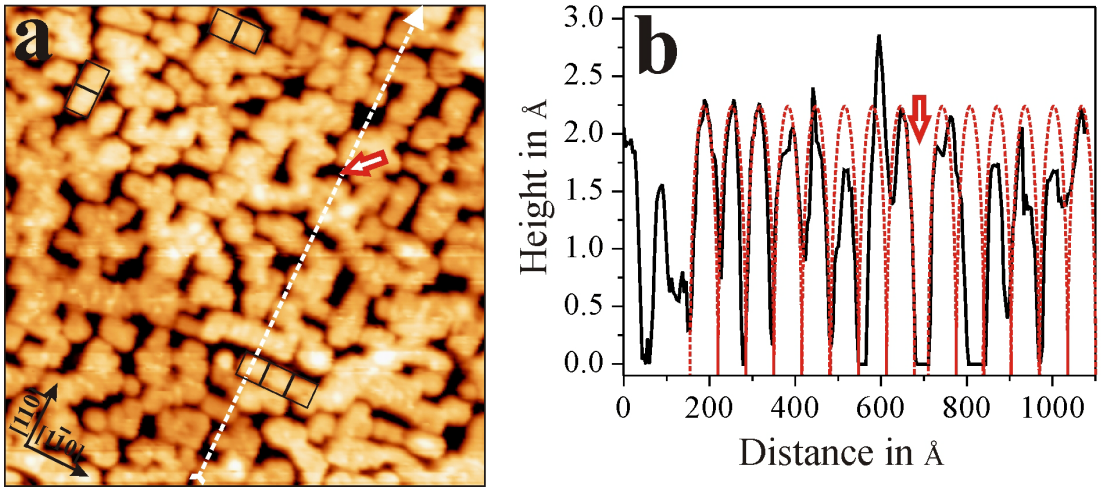

Fig.2: (a) STM image of a sub-monolayer MgO/Mo(001) film (U_s = 4.0 V, 90 × 90 nm^2). The MgO forms rectangular islands that seem to be composed of unit squares with 55 × 55 Å^2 size (see black squares). **(b)** The regularity of the island pattern becomes evident in the height profile taken along the Mo[110] direction. Apart from a boundary marked by the arrow, the islands are spaced by (55 ± 5) Å, as visualized by the overlaid periodic function (red curve).

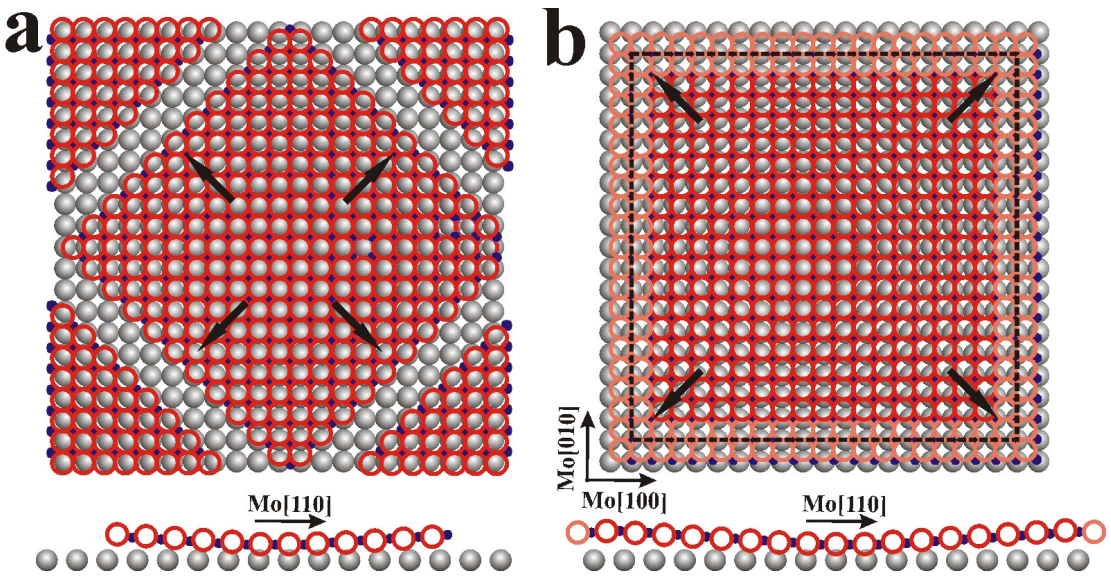

Fig.3: (a) Structure model of a sub-monolayer MgO/Mo(001) film, top view and [110]-oriented side view. The O and Mg ions are depicted with large-red and small-violet spheres, respectively, the substrate Mo atoms are shown in grey. The distinct square shape of the islands results from the preferential formation of O-Mo bonds at the interface. **(b)** Structure model of a monolayer MgO/Mo(001) film. Due to the lattice mismatch, the film forms a coincidence structure with 56 Å edge length. Whereas in the center of the coincidence cell, O-Mo interfacial bonds are formed, the registry shifts towards Mg-Mo bonds at the corner and edges of the unit cell. The associated tilt of the oxide plane is depicted by arrows.

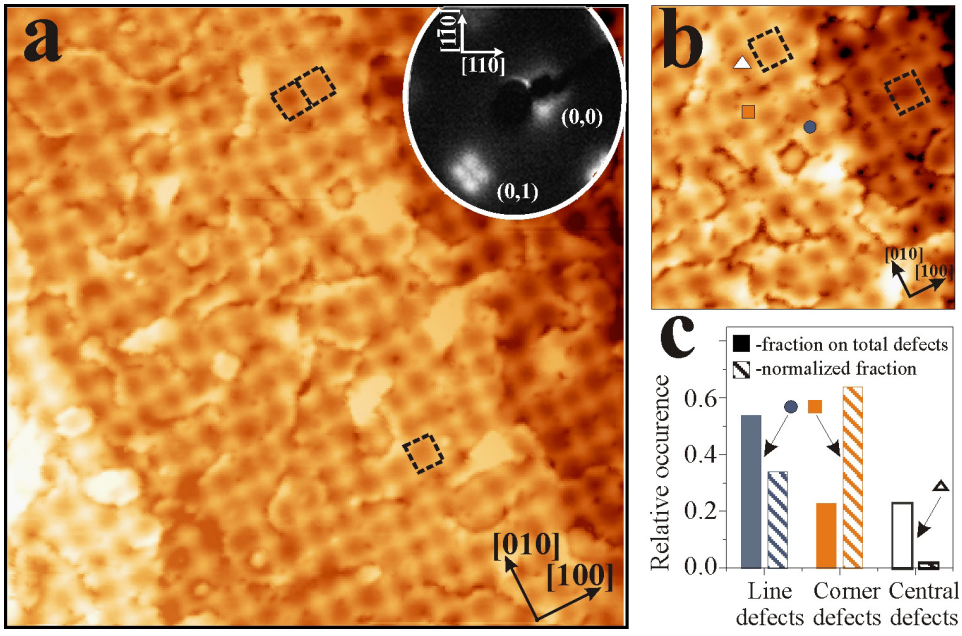

Fig.4: (a) STM image and LEED pattern (55 eV) of a monolayer MgO/Mo(001) film showing the typical square pattern (U_s = 3.5 V, 100 × 100 nm^2). The coincidence cell is marked by dashed lines. **(b)** MgO surface with point and line defects. According to their position in the coincidence cell, the point defects are classified into corner (square), line (circles) and center defects (triangles). **(c)** Fraction of the three defect types on the total number of defects (solid boxes) and normalized with the number of sites in the respective oxide regions (striped boxes). In total, 521 defects in an area of 140×140 nm^2 have been considered for the statistics.

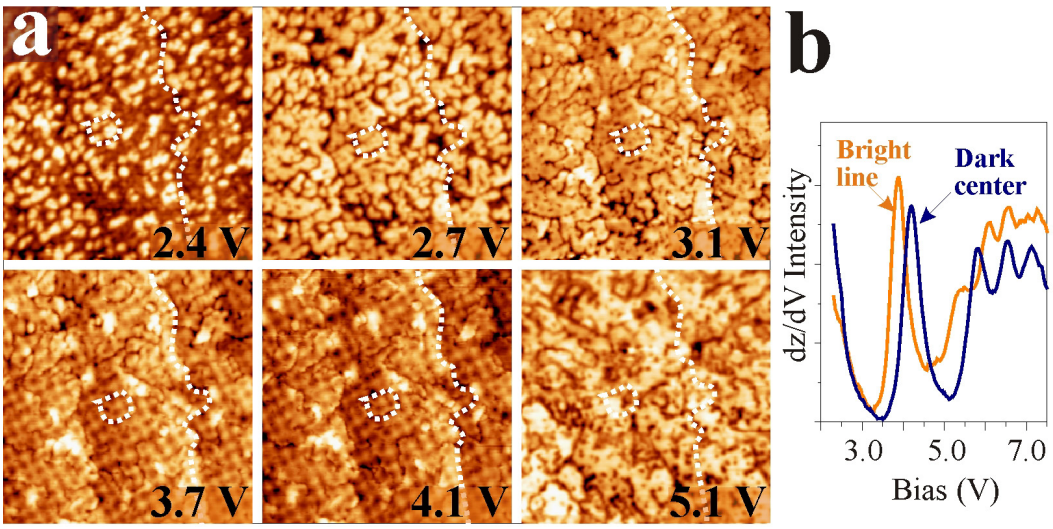

Fig. 5: (a): STM bias series of an identical MgO/Mo(001) region (100 × 100 nm^2). The dashed lines mark selected domain boundaries and should serves as guides to the eye. The characteristic square pattern is only visible in a small bias range around 4.0 V. **(b)** dz/dV spectra taken above a bright and a dark region of the coincidence pattern. The first FER is clearly down-shifted above the bright lines compared to the center of the coincidence cell.

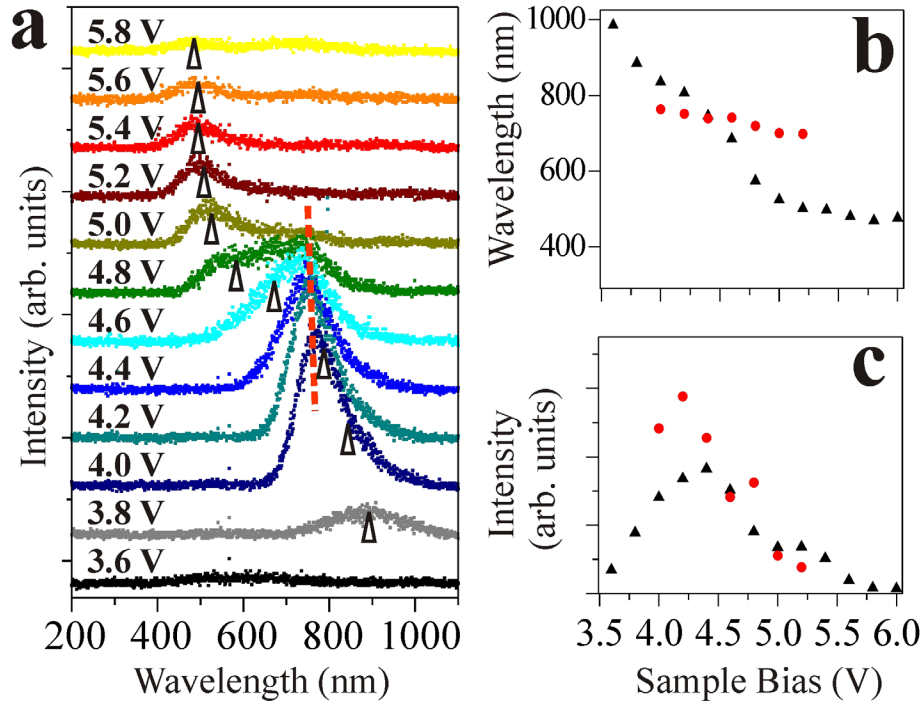

Fig.6: (a) Photon emission spectra taken as a function of excitation bias on a monolayer MgO/Mo film (current: 2nA, accumulation time: 120 s). Two spectral contributions are discernable: The one marked by the triangles continuously blue-shifts with increasing bias and is assigned to a tip-induced plasmon (TIP). The one depicted by the broken line appears at constant wavelength and relates to radiative electron transitions involving FERs in front of the MgO surface. **(b)** Peak position and **(c)** emitted intensity of the two spectral contributions. The TIP mode (black triangles) shows maximum intensity around 4.5 V, when the field enhancement between tip and

sample is large. The FER-mediated emission (red spheres) is confined to the bias range where electrons from the tip are able to populate the first FER.

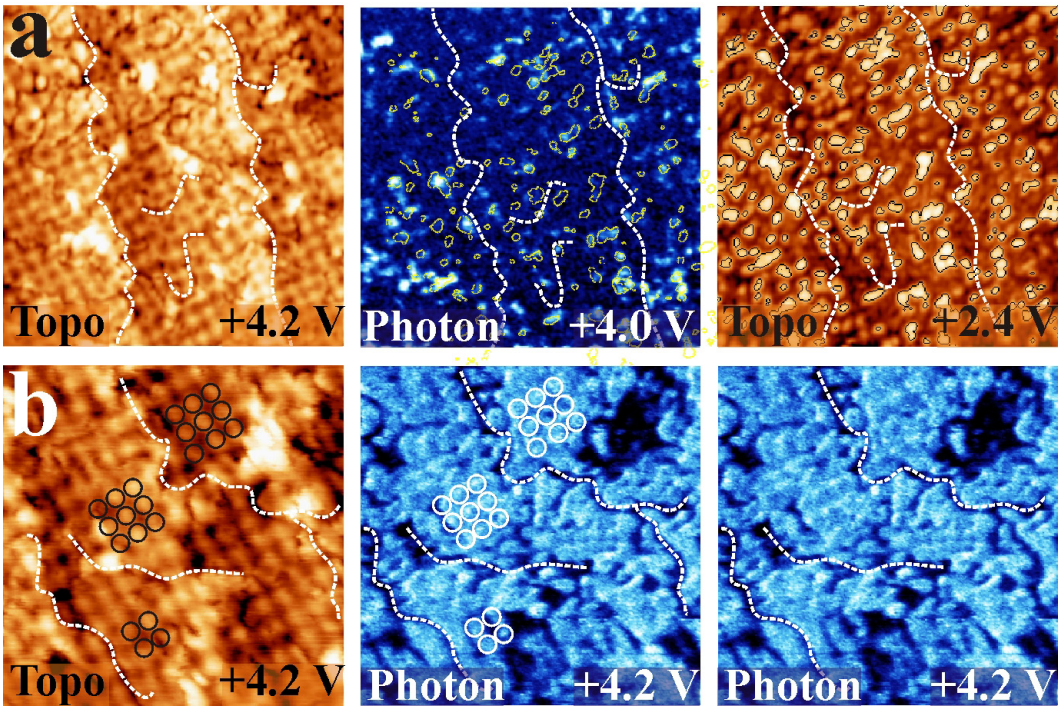

Fig.7: (a) Topographic image and photon map of a thin MgO/Mo(001) film taken at the indicated bias voltage (2 nA, 100 × 100 nm^2). The dominant emission channel is the decay of TIP modes and the emitted intensity follows the final-state-density probed by the inelastic electrons. The emission centers in the surface therefore match the regions with high oxide LDOS at (eV_o-$\hbar\omega_{TIP}$), as corroborated by the topographic image on the right. The dashed lines mark domain boundaries in the film and should serve as guides to the eye. **(b)** Topographic image and photon maps of a thin MgO/Mo(001) film (2 nA, 70 × 70 nm^2). At the chosen bias-conditions, the FER-mediated mechanism strongly contributes to the light emission. Whereas the original photon map is depicted in the right panel, characteristic structural elements of the film are overlaid in the central one.

[1] M. Bäumer and H.-J. Freund, Progr. Surf. Sci. 61 (1999) 127.
[2] S. A. Chambers, Surf. Sci. Rep. 39 (2000) 105; C. T. Campbell, Surf. Sci. Rep. 27 (1997) 1.
[3] W. Weiss and W. Ranke, Prog. Surf. Sci. 70 (2002) 1.
[4] J. Goniakowski and C. Noguera, Interface Sci. 12 (2004) 93.
[5] L. Giordano and G. Pacchioni, PhysChemChemPhys 8 (2006) 3335.
[6] L. Giordano, G. Pacchioni, J. Goniakowski, N. Nilius, E. D. L. Rienks and H.-J. Freund, Phys. Rev. B 76 (2007) 075416.
[7] J. L. Vassent, M. Dynna, A. Marty, B. Gilles and G. Patrat, J. Appl. Phys. 80 (1996) 5727.
[8] S. Benedetti, H. M. Benia, N. Nilius, S. Valeri and H.-J. Freund, Chem. Phys. Lett. 430 (2006) 330.
[9] M. Schmid, M. Shishkin, G. Kresse, E. Napetschnig, P. Varga, M. Kulawik, N. Nilius, H.-P. Rust and H.-J. Freund, Phys. Rev. Lett. 97 (2006) 046101.
[10] G. Renaud, P. Guénard and A. Barbier, Phys. Rev. B 58 (1998) 7310.

[11] J. Wollschläger, D. Erdos, H. Goldbach, R. Hopken and K. M. Schröder, Thin Solid Films 400 (2001) 1.
[12] C. Hagendorf, R. Shantyr, H. Neddermeyer and W. Widdra, PhysChemChemPhys 8 (2006) 1575.
[13] T. Orzali, S. Agnoli, M. Sambi and G. Granozzi, Surf. Sci. 569 (2004) 105.
[14] S. Valeri, S. Benedetti and P. Luches, J. Phys. Cond. Matt. 19 (2007) 225002.
[15] P. Luches, V. Bellini, S. Colonna, L. Di Giustino, F. Manghi, S. Valeri and F. Boscherini, Phys. Rev. Lett. 96 (2006) 106106.
[16] G. Kresse, M. Schmid, E. Napetschnig, M. Shishkin, L. Köhler and P. Varga, Science 308 (2005) 1440.
[17] C. Hagendorf, S. Sachert, B. Bochmann, K. Kostov and W. Widdra, Phys. Rev. B 77 (2008) 075406.
[18] J. Schoiswohl, W. Zheng, S. Surnev, M. G. Ramsey, G. Granozzi, S. Agnoli and F. P. Netzer, Surf. Sci. 600 (2006) 1099.
[19] S. Schintke, S. Messerli, M. Pivetta, F. Patthey, L. Libjoulle, M. Stengel, A. de Vita and W. D. Schneider, Phys. Rev. Lett. 87 (2001) 276801.
[20] H. M. Benia, P. Myrach and N. Nilius, New J. Phys. 10 (2008) 013010.
[21] E. D. L. Rienks, N. Nilius, H.-P. Rust and H.-J. Freund, Phys. Rev. B 71 (2005) 241404.
[22] M. C. Gallagher, M. S. Fyfiled, L. A. Bumm, J. P. Cowin and S. A. Joyce, Thin Solid Films 445 (2003) 90.
[23] S. Benedetti, P. Torelli, S. Valeri, H. M. Benia, N. Nilius and G. Renaud, Phys. Rev. B 78 (2008) 195411.
[24] H. M. Benia, N. Nilius and H.-J. Freund, Surf. Sci. Lett. 601 (2007) L55.
[25] L. Giordano, F. Cinquini and G. Pacchioni, Phys. Rev. B 73 (2005) 045414.
[26] G. Pacchioni, L. Giordano and M. Baistrocchi, Phys. Rev. Lett. 94 (2005) 226104.
[27] M. Sterrer, T. Risse, U. Martinez Pozzoni, L. Giordano, M. Heyde, H.-P. Rust, G. Pacchioni and H.-J. Freund, Phys. Rev. Lett. 98 (2007) 096107.
[28] S. Sicolo, L. Giordano, G. Pacchioni, J. Phys. Chem. C 113 (2009) 16694.
[29] N. Nilius, A. Cörper, G. Bozdech, N. Ernst and H.-J. Freund, Prog. Surf. Sci. 67 (2001) 99.
[30] M. C. Wu, J. Corneille, C. Estrada, J.-W. He and D. W. Goodman, Chem. Phys. Lett. 182 (1991) 472.
[31] K. Honkala and H. Häkkinen, J. Phys. Chem. C. 111 (2007) 4319.
[32] S. Benedetti, P. Luches, M. Liberati and S. Valeri, Surf. Sci. 572 (2004) L348.
[33] H. M. Benia, *Doctoral thesis*, (Humboldt University, Berlin, 2008).
[34] I. Sebastian and H. Neddermeyer, Surf. Sci. 454 (2000) 771.
[35] K. H. Hansen, T. Worren, E. Laegsgaard, F. Besenbacher and I. Stensgaard, Surf. Sci. 475 (2001) 96.
[36] G. Binnig, K. H. Frank, H. Fuchs, N. Garcia, B. Reihl, H. Rohrer, F. Salvan and A. R. Williams, Phys. Rev. Lett. 55 (1985) 991.
[37] O. Y. Kolesnychenko, Y. A. Kolesnichenko, O. I. Shklyarevskii and H. van Kempen, Physica, B 291 (2000) 246.
[38] J. Zhu, J. A. Farmer, N. Ruzycki, L- Xu, C. T. Campbell and G. Henkelman, J. Am. Chem. Soc. **130** (2008) 2314.
[39] J. Goniakowski, C. Noguera, Phys. Rev. B 79 (2009) 155433.
[40] R. Berndt, in: R. Wiesendanger (Ed.), Scanning Probe Microscopy, Springer Series Nanoscience and Technology, (Springer, Berlin, 1998) p97.
[41] P. Johansson, R. Monreal and P. Apell, Phys. Rev. B 42 (1990) 9210.
[42] G. V. Nazin, X. H. Qui and W. Ho, Phys. Rev. Lett. 90 (2003) 216110.
[43] N. Nilius, E. Rienks, H.-P. Rust and H.-J. Freund, Phys. Rev. Lett. 95 (2005) 066101; X. Lin and N. Nilius, J. Phys. Chem. C 112 (2008) 15325.